RESEARCH ARTICLE

Design and Kinematic Analysis of a Novel Planar Parallel Robot With Pure Translations

QI ZOU[1], BYUNG-JU YI[1], (Member, IEEE), DAN ZHANG[2], (Senior Member, IEEE), YUANCHENG SHI[1], AND GUANYU HUANG[3]

[1]School of Electrical Engineering, Hanyang University, Ansan-si 15588, South Korea
[2]Department of Mechanical Engineering, The Hong Kong Polytechnic University, Hong Kong, China
[3]Zhejiang Laboratory, Intelligent Robotics Research Center, Hangzhou 311121, China

Corresponding authors: Byung-Ju Yi (bj@hanyang.ac.kr) and Dan Zhang (dan.zhang@polyu.edu.hk)

ABSTRACT The structural synthesis of a group of parallel mechanisms can be established by an exhaustive enumeration of all feasible kinematic chains based on the screw theory. However, reliable kinematic limbs can provide mobility constraints for some unqualified supporting legs to guarantee the degrees-of-freedom feasibility of the parallel robots. A systematic design approach is presented for a family of planar single-loop parallel mechanisms with the consideration of infeasible kinematic chains. Different from the other design approaches for single-loop linkages, the fixed and moving platforms are predefined in this research to distinguish different kinematic limbs. The special parallelogram linkage mechanism is incorporated due to its equivalent translation capacity. Three categories of singularity configurations are investigated based on the detailed kinematic models. The reachable workspace is obtained through the spatial search methodology. Several novel kinematic error model associated performance indices are proposed in this work and examined on a translational parallel manipulator. Experiments are carried out and compared to testify the effectiveness of the kinematic analysis and proposed position-based controller.

INDEX TERMS Parallel robot, planar mechanism, type synthesis, performance measurement.

I. INTRODUCTION

A parallel robot is generally constituted of several kinematic chains connecting the fixed base and mobile platform. It tends to have higher speed, acceleration, stiffness and payload capacity, lower inertia property, at the cost of limited reachable workspace and many singularity configurations, by comparison with its counterpart serial robot in the similar conditions [1], [2]. Parallel manipulators have received increased interest due to their intrinsic advantages and are widely employed in various industrial applications: pick-and-place robots [3], [4], flight simulators [5], multi-axis parallel kinematic machine tools [6], [7], haptic devices [8] and medical robots [9].

The associate editor coordinating the review of this manuscript and approving it for publication was Yangmin Li.

A systematic design of a group of novel parallel architectures is the primary step in robotics. There are four main type synthesis methodologies: generalized function set theory, single open chain approach, the theory of screw, Lie group and Lie algebra [10], [11], [12], [13], [14]. The screw theory has been utilized in many research. Inspired by the parallel module of the five-axis machine tool Exechon with over-constraint [15], a general parallel manipulator with the same kind of 1T2R (T represents translation and R denotes rotation) motion was created. Screw theory was employed to synthesize a family of feasible kinematic limbs, based on which, 24 asymmetrical parallel structures with two categories of chains were obtained and examined. The refined virtual chain methodology based on screw theory was developed in [16]. Screw theory was employed to identify the constraint screw system for each kinematic limb and

then the maximal number of kinematic joints in each limb. A family of qualified kinematic branches was obtained. The feasible mechanisms were generated by the elimination of special joints in some virtual limbs and the combination of two adjacent rods with the same movements. The authors in [17] computed the wrench systems for the mobile platform and kinematic limbs of 2R1T parallel architectures. The total number and types of joints were explored for kinematic chains. The desired parallel manipulators with three or four branches were separately introduced by enumerating all possible chains with a minimal number of kinematic pairs. A kind of deployable parallel structure was divided into two sub-mechanisms, grasping and auxiliary modules [18]. The twist system of the grasping module was employed to obtain the wrench system of the auxiliary module. The auxiliary module was first synthesized, which led to the identification of possible grasping linkages. Yi and Kim [19] reported two levels of the constraint-based type synthesis approach for parallel architectures. The detailed procedures were summarized and testified by three categories of planar parallel structures consisting of symmetrical and asymmetrical configurations. Fomin et al. [20] employed the screw theory to testify the mobility of a family of FoldRail parallel mechanisms. The spherical motion and unfolding screw motion of two selected mechanisms with three kinematic limbs were also revealed by the screw theory.

Performance evaluation is important for parallel robotics. Patel and Sobh [21] had conducted a comprehensive survey of performance indices, which could be divided as local or global measurements, kinematics-based or dynamics-based indicators or neither, intrinsic or extrinsic indices, in regard to pose range, performance features, and application, respectively. However, most of them were associated with the kinematic Jacobian matrix. The motion/force transmission indices incorporating both movement and force/torque transmission properties [22], [23], should be considered as supplementary measurements besides Jacobian-matrix-based indicators before manufacturing a physical prototype.

There are two concerns in utilizing a Jacobian matrix. On the one hand, the indices (i.e., local condition index) requiring the inverse matrix of a Jacobian matrix can be an issue when it comes to non-square Jacobian matrices of some parallel manipulators, especially parallel mechanisms with kinematic or actuation redundancy [24], [25]. A common solution is to employ the pseudo-inverse matrix instead of the inverse matrix [26], [27].

On the other hand, the non-homogeneous units of translational and rotational movements in some parallel manipulators reduce the feasibility of these indices [28], [29]. The first solution is to employ dimensionless/normalized variables. For example, Khan and Angeles [30] created a homogeneous line to assist the construction of homogeneous Plücker coordinates. The condition number based on the homogeneous Jacobian matrix was reported and examined.

It is noteworthy that the indices based on the screw theory are intrinsically dimensionless. The asymmetrical parallel robot 2RPU-RPS-UPS (P, R, U and S respectively represent prismatic, revolute, universal and spherical joints) was proposed in [31]. Based on the global coordinate system, the twist screw for every kinematic joint was computed. The local transmission index was formulated with the calculations of input and output transmission indicators. According to the foundation of the power coefficient, Liu et al. [32] outlined three constraint indicators for parallel mechanisms, input, output and total constraint indicators. Their performance distributions for the symmetrical 3-PRS and asymmetrical 3-UPS/UP mechanisms were explored, respectively. The authors in [33] further expanded the conventional output transmission index to be applicable for parallel manipulators with articulated platforms. The medial transmission index was also outlined to evaluate the relative movement between the two travelling plates. The modified local transmission index was reported to measure the motion/force transmission features of these kinds of mechanisms. Sharafian et al. [34] provided detailed calculation procedures for constraint transformation matrices of parallel manipulators in accordance with three approaches (two joint-based and one rod-based). Three strategies were investigated and compared on two different linkage mechanisms. Xu and Li [35] proposed the translational parallel structure 3-PRC (C indicates cylindrical joint). Its complete stiffness model was established via the screw theory with the consideration of active prismatic joints, geometrical conditions, and linkage compliances. In the work of [36], the pose-related energy was invented by the virtual work principle and screw theory, based on which the new instantaneous stiffness indicator was proposed without the concern of inconsistent linear/angular units. This index's distribution of the 3-UPS/UPP parallel mechanism was explored.

The second solution is to split the translational and rotational indicators to keep homogeneous physical units. Cardou et al. [26] mentioned that the most popular indices for serial/parallel robots were on the foundation of the manipulability index and condition number. Considering the complexity of developing a unified index with different units, the authors separately proposed two indices for linear and angular variables to measure the kinematic sensitivity.

The 2-translation planar parallel manipulators (i.e., 2-PRR [37] and 2-RRR [38]) have gained increasing interest due to the simplicity of structures and mathematical modeling. The simple and reliable structure of this kind of parallel mechanisms facilitates the decoupled motions and control strategy design when integrated into a hybrid industrial robot aiming for complicated operation, e.g., Diamond mechanism [39], [40], PRR-PPa [41], special planar mechanism with 3 Parallelogram joints (P_a) [42]. Liu et al. [43] proposed a planar parallel robot with symmetric kinematic chains. The mobile platform remained a constant orientation by using a parallelogram linkage in each limb.

This design was further integrated into a five-axis machine tool. Pham and Kim [44] developed a 2-DOF parallel manipulator. This robot consisted of two active prismatic joints with orthogonal directions.

To satisfy the requirements in many industrial applications, simple parallel robot designs are still in need that can mitigate the intrinsic issues (e.g., complicated mathematical models, limited workspace, singularities) of parallel manipulators. It is still a challenging task to further investigate issues of structural synthesis and performance measures. It is not mentioned in the past research that the infeasible kinematic joints/chains identified by the mechanism design approaches can still be utilized to construct required parallel structures. It is also essential to expand the indices family to establish more comprehensive assessments for parallel mechanisms, especially about kinematic error sensitivity with consistent physical units. The layout of this paper is organized as follows: A systematic design approach for planar translational parallel structures considering infeasible joints is presented in Section II. The complete analytical inverse and forward kinematic models of the selected mechanism are constructed in Section III. In Section IV, the detailed kinematic features of this parallel robot are explored. Several novel indices pertinent to the kinematic error mathematical model are developed and examined for the chosen parallel architecture. A circular path is performed in the experiments under two conditions in Section V, followed by Section VI which summarizes this research.

II. STRUCTURAL SYNTHESIS OF A FAMILY OF 2T PARALLEL MECHANISMS

The motion of the mobile platform is confined by the pure constraint forces/torques from all kinematic limbs for most parallel mechanisms [17]. The constraints of a translational parallel structure can be expressed as

$$_m\$^r = \{_{m,1}\$^r, _{m,2}\$^r, _{m,3}\$^r, \ldots, _{m,\sigma}\$^r\}$$
$$= \mathrm{U}_{i=1}^{j}\{\$_{i,1}^r, \$_{i,2}^r, \$_{i,3}^r, \ldots, \$_{i,\zeta}^r\} \quad (1)$$

where the subscript m denotes the mobile platform and the superscript r indicates the reciprocal screw. The subscript σ means the sum of reciprocal screws for the traveling plate, and its maximal number is 5 if all constraint wrenches in the curly brackets are linearly independent. The superscript j and subscript i, ζ are respectively the total number of kinematic chains and all reciprocal screws of the i-th kinematic chain.

It is assumed that the planar translational parallel manipulator has two kinematic branches and is placed in the XOY plane in 3-dimensional space. In this case, there are four linearly independent constraint wrenches (three constraint couples and one constraint force) exerted on the mobile platform. Every two couples are orthogonal and one couple among them is parallel to Z direction. The constraint force is parallel to Z axis. Henceforth, the largest number ζ for linear independent wrenches is four for any kinematic branch. The minimal degrees-of-freedom (DOFs) sum of kinematic joints

in each kinematic leg can be calculated as 6-4=2, since there are six linear independent screws in total. In other words, there will be at least two kinematic joints with single degree-of-freedom in any kinematic limb. The twist screw system of the mobile platform can be derived as the reciprocal screws of (1)

$$_m\$ = \{_{m,1}\$, _{m,2}\$\}$$
$$= \{[0\ 0\ 0;\ 1\ 0\ 0]^T, [0\ 0\ 0;\ 0\ 1\ 0]^T\} \quad (2)$$

Equation (2) can also be regarded as the intersection of the corresponding kinematic screw systems of all kinematic chains.

The wrench system of the moving platform can be further written as

$$_m\$^r = \{[s_F;\ r_F \times s_F]^T, [0;\ s_{C,1}]^T,$$
$$[0;\ s_{C,2}]^T, [0;\ s_{C,3}]^T\} \quad (3)$$

where the subscripts F and C represent the constraint force and constraint couple, respectively.

The next step is to search for the qualified kinematic joints. The prismatic and revolute joints are considered in this group of parallel mechanisms. The parallelogram joint is employed by the merit of translational motion and is regarded as a special kinematic pair. Their corresponding kinematic screws are listed as

$$\begin{cases} \$_P = [0;\ s_P]^T \\ \$_R = [s_R;\ r_R \times s_R]^T \\ \$_{Pa} = [0;\ s_{Pa}]^T \end{cases} \quad (4)$$

where the subscripts P, R and Pa denote prismatic, revolute and parallelogram joints, respectively.
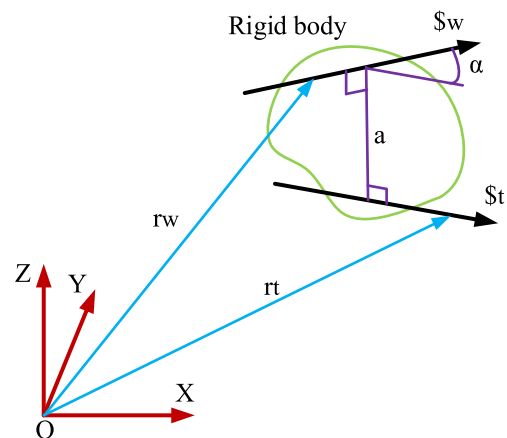

FIGURE 1. Schematic diagram of the screw system on a rigid body.

The twist and wrench of one rigid linkage can be seen in Fig. 1. The wrench $\$_w$ and twist $\$_t$ can represent any screw in (3) and (4) respectively. r_w and r_t respectively mean the corresponding position vector from the origin to any dot in the direction of these two screws. The distance a is measured

in the common perpendicular line of two screws. This line is also utilized as the axis to calculate the rotational angle between these two screws.

A kinematic joint in (4) will be qualified in any chain if all constraints of (3) can generate zero virtual work in all poses within the workspace. This leads to

$$
\begin{cases}
s_P \cdot s_F = \cos \alpha_1 = 0 \\
\$_P \circ \begin{bmatrix} 0; & s_{C,1} \end{bmatrix}^{\mathrm{T}} \equiv 0 \\
\$_P \circ \begin{bmatrix} 0; & s_{C,2} \end{bmatrix}^{\mathrm{T}} \equiv 0 \\
\$_P \circ \begin{bmatrix} 0; & s_{C,3} \end{bmatrix}^{\mathrm{T}} \equiv 0
\end{cases}
\tag{5}
$$

$$
\begin{cases}
s_R \cdot (r_F \times s_F) + s_F \cdot (r_R \times s_R) = -a_2 \sin \alpha_2 = 0 \\
s_R \cdot s_{C,1} = \cos \alpha_3 = 0 \\
s_R \cdot s_{C,1} = \cos \alpha_4 = 0 \\
s_R \cdot s_{C,1} = \cos \alpha_5 = 0
\end{cases}
\tag{6}
$$

$$
\begin{cases}
s_{Pa} \cdot s_F = \cos \alpha_6 = 0 \\
\$_{Pa} \circ \begin{bmatrix} 0; & s_{C,1} \end{bmatrix}^{\mathrm{T}} \equiv 0 \\
\$_{Pa} \circ \begin{bmatrix} 0; & s_{C,2} \end{bmatrix}^{\mathrm{T}} \equiv 0 \\
\$_{Pa} \circ \begin{bmatrix} 0; & s_{C,3} \end{bmatrix}^{\mathrm{T}} \equiv 0
\end{cases}
\tag{7}
$$

where $\alpha_i (i = 1, 2, \ldots, 6)$ means the angle between the corresponding twist and wrench screws. The symbol $\circ$ is for reciprocal product operation and $\equiv$ is the identity sign.

On the basis of (5), the direction of feasible prismatic joint should be perpendicular to the constraint force. Three constraint couples cause no limitation for prismatic joints since the latter three equations are equal to zero inherently. According to the first expression of (6), the axis of the qualified revolute joint should intersect with the axis of the constraint force or be parallel to this force. The rotary joint will not exist since it is required to be orthogonal with all three constraint couples (this geometric relationship doesn't exist in 3D space) based on the remaining expressions of (6). The parallelogram joint case has the same conditions as the prismatic joint because of the similar expressions between (5) and (7).
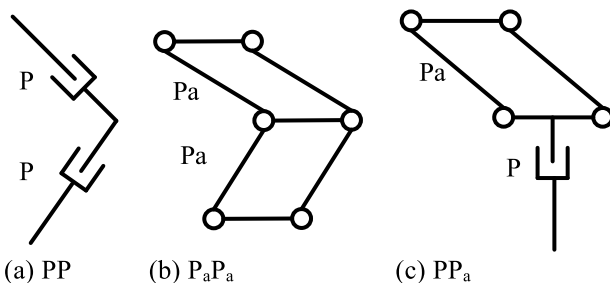

FIGURE 2. Diagrams of feasible branches of two joints (Various orientations of P joints indicate different P joints axes).

Therefore, the feasible kinematic chains and parallel mechanism structures can be found on the basis of the

above calculations. The components (kinematic joints) combinations instead of permutations are employed in each kinematic chain for simplification. The first group of qualified kinematic limbs incorporates two kinematic pairs. The possible kinematic branches in the XOY plane include PP, P_aP_a and PP_a, as denoted in Fig. 2. It is noteworthy that two prismatic joints can not be collinear for the purpose of this chain's planar translation requirement. The proper parallel structures can be explored through the cooperation of two promising branches. The corresponding parallel architectures are illustrated in Fig. 3 (The mobile platform is illustrated as a green rod. The P joint can point any direction in XOY plane, as long as two successive P joints in one kinematic chain are not parallel.).

It is noteworthy that all parallel mechanisms in Fig. 3 possess two planar DOFs and four kinematic joints, while they do not belong to the commonly seen four-bar linkages (one-DOF in general cases). In accordance with the constraint system (three constraint couples and one constrain force) for the moving platform described in the second paragraph of this section, the common constraint and order of these mechanisms are 4 and 6-4=2, respectively. The mobility of these structures is 2 according to the modified Grübler-Kutzbach formula. The sum of motions of the mobile platform is equal to the mechanism's mobility for any case in Fig. 3.

There are three kinematic joints in each chain for the second group of parallel manipulators. Based on the aforementioned selection criteria, the reliable kinematic chains are composed of PPP, $P_aP_aP_a$, PP_aP_a and P_aPP, as provided in Fig. 4. The only special case is Fig. 4(a) where three joints are not supposed to be parallel to each other in any circumstance.

The promising parallel structures can be generated in a similar manner, as depicted in Fig. 5.

Considering the feasibility of kinematic chains in the first and second groups, the parallel mechanisms integrated with two groups of chains can meet the motion requirement. The third family of cases is shown in Table 1 to save length.

TABLE 1. The third group of parallel mechanisms.

PP-PPP	PP-PaPaPa	PP-PPaPa	PP-PaPP
PaPa-PPP	PaPa-PaPaPa	PaPa-PPaPa	PaPa-PaPP
PPa-PPP	PPa-PaPaPa	PPa-PPaPa	PPa-PaPP

The proposed planar parallel mechanisms with two chains belong to single-loop mechanism, just like the linkages in [45]. However, there are three different points. At first, the special kinematic joint P_a is employed in this class of mechanisms, which expands the possible kinematic limbs and parallel architectures. Secondly, there are predefined base and moving platforms.

The uniqueness of parallel structures can be guaranteed. For example, $P_aP_aP_a$-P_aPP and PP_aP_a-PP_aP_a represent-
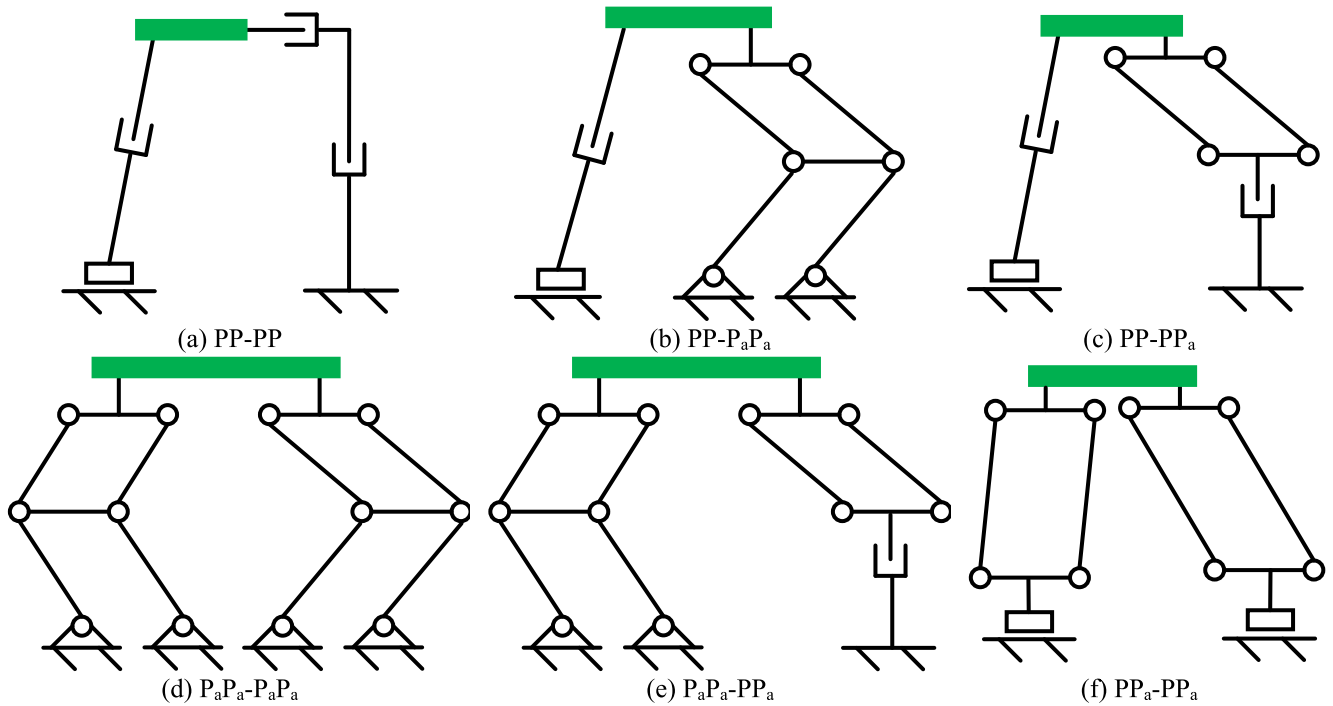
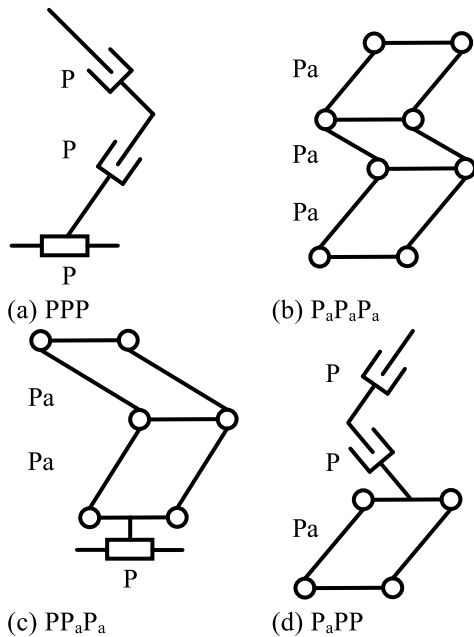**FIGURE 3.** Illustrations of planar parallel manipulators.

FIGURE 4. Diagrams of kinematic chains with three joints.

ing various parallel structures are regarded as the same $P_aP_aP_aP_aPP$ single-loop linkage based on the definition in [45]. Thirdly, the infeasible joint condition can still exist in one kinematic chain of a desired parallel manipulator, while the other chain must completely obey the aforementioned rules (at least two DOFs of this kinematic chain and meet the criteria (5)-(7)). This merit leads to the last category of

practical mechanisms where the revolute joint is utilized. The possible kinematic limbs (they belong to unqualified supporting legs due to (6) include RRR, PRR, RPP, RP_aP_a, P_aRR and PRP_a, as depicted in Fig. 6.

Different from the first and second categories of parallel mechanisms, the combination of kinematic branches in this group leads to additional rotational movement for the mobile platform. Therefore, this category of parallel robots can be enumerated by combining branches in Fig. 6 with limbs in Fig. 2 or Fig. 4, as summarized in Table 2.

Although the above calculations demonstrate that at least two DOFs in each chain are suitable for planar two translations, parallel manipulators with six joints in one closed loop will require more than two motors for expected movement. Hence, kinematic chains with more than three kinematic joints (single DOF) are beyond the scope of this study. The workflow of the type synthesis methodology based on the screw theory is summarized in Fig.7. It is noteworthy that the type synthesis approach can be utilized for the design of parallel manipulators with more (3 to 6) DOFs.

III. ANALYTICAL KINEMATIC MODELS

The novel parallel robot represented in Fig. 3(f) is selected according to its simple and symmetrical structure. One special case with two identical chains is shown in Fig. 8. The coordinate frame O-XYZ attached to the fixed platform is constructed. The actuation joints of two kinematic branches are colinear with X axis.
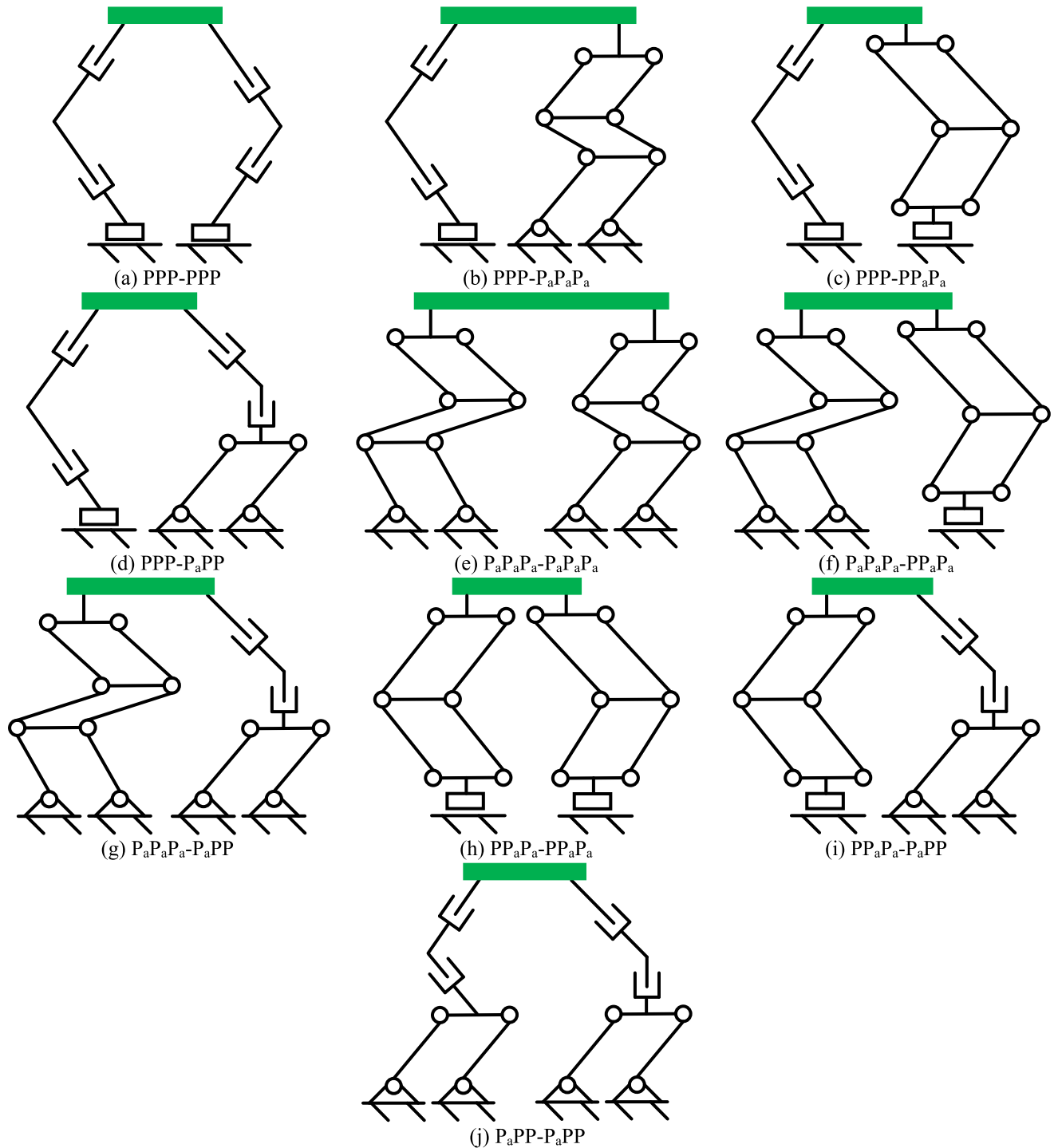
FIGURE 5. Reliable parallel mechanisms with six joints.

It is noted that points A_i, B_i ($i = 1,3$) are in the X axis (the offset along the Y-direction between A_i (or B_i) and the X axis is ignored in Fig.8). Points A_j, B_j ($j = 2,4$) and P have the same height along Y axis (the offset along the Y-direction between A_j (or B_j) and point P is ignored in Fig.8). The midpoints of rods A_1A_3, A_2A_4, B_1B_3 and B_2B_4 are respectively indicated as A_5, A_6, B_5 and B_6. The stroke of

the two prismatic joints is L_1. The dimensions of rods A_1A_2 or (A_3A_4) and A_1A_3 or (A_2A_4) are L_2 and $2L_3$, respectively. The linkage dimensions of B_1B_2 or (B_3B_4) and B_1B_3 or (B_2B_4) are separately L_4 and $2L_5$. L_6 is defined as the distance between point P and point A_4 (or B_2) along the X direction. θ_1 and θ_2 separately present the sloping angles for rods A_3A_4 and B_3B_4, regarding to the positive X axis.

TABLE 2. The fourth classes of parallel mechanisms.

PP-RRR	PP-PRR	PP-RPP	PP-RP$_a$P$_a$	PP-P$_a$RR	PP-PRP$_a$
P$_a$P$_a$-RRR	P$_a$P$_a$-PRR	P$_a$P$_a$-RPP	P$_a$P$_a$-RP$_a$P$_a$	P$_a$P$_a$-P$_a$RR	P$_a$P$_a$-PRP$_a$
PP$_a$-RRR	PP$_a$-PRR	PP$_a$-RPP	PP$_a$-RP$_a$P$_a$	PP$_a$-P$_a$RR	PP$_a$-PRP$_a$
PPP-RRR	PPP-PRR	PPP-RPP	PPP-RP$_a$P$_a$	PPP-P$_a$RR	PPP-PRP$_a$
P$_a$P$_a$P$_a$-RRR	P$_a$P$_a$P$_a$-PRR	P$_a$P$_a$P$_a$-RPP	P$_a$P$_a$P$_a$-RP$_a$P$_a$	P$_a$P$_a$P$_a$-P$_a$RR	P$_a$P$_a$P$_a$-PRP$_a$
PP$_a$P$_a$-RRR	PP$_a$P$_a$-PRR	PP$_a$P$_a$-RPP	PP$_a$P$_a$-RP$_a$P$_a$	PP$_a$P$_a$-P$_a$RR	PP$_a$P$_a$-PRP$_a$
P$_a$PP-RRR	P$_a$PP-PRR	P$_a$PP-RPP	P$_a$PP-RP$_a$P$_a$	P$_a$PP-P$_a$RR	P$_a$PP-PRP$_a$
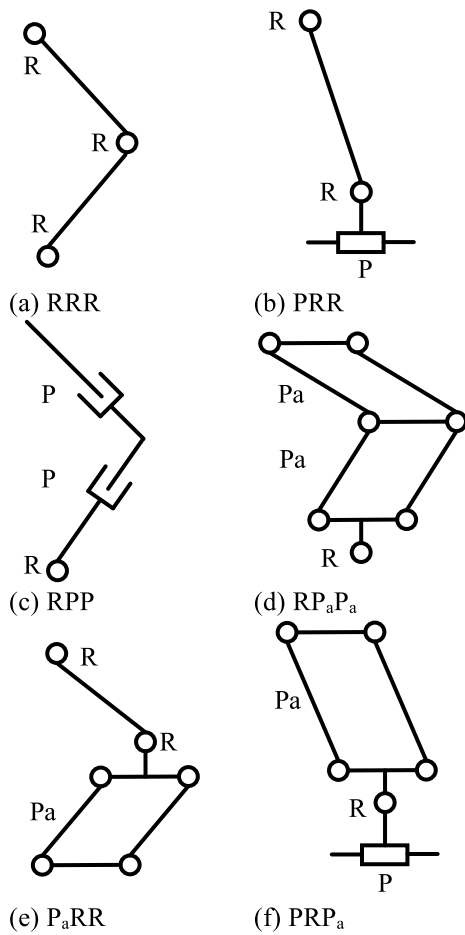
FIGURE 6. The feasible kinematic limbs with R joint.

FIGURE 7. Workflow of the type synthesis approach.

The positions of two actuating joints are denoted as $Q = [x_{A5}, x_{B5}]^T$. The location of the moving platform is defined as $X = [x_P, y_P]^T$. The positions of some points are provided as $P_{A5}(x_{A5}, 0)$, $P_{A6}(x_P - L_3 - L_6, y_P)$, $P_{B5}(x_{B5}, 0)$, $P_{B6}(x_P + L_3 + L_6, y_P)$, respectively.

For the analytical inverse kinematic model, the closed-loop formula of the first kinematic chain can be solved as
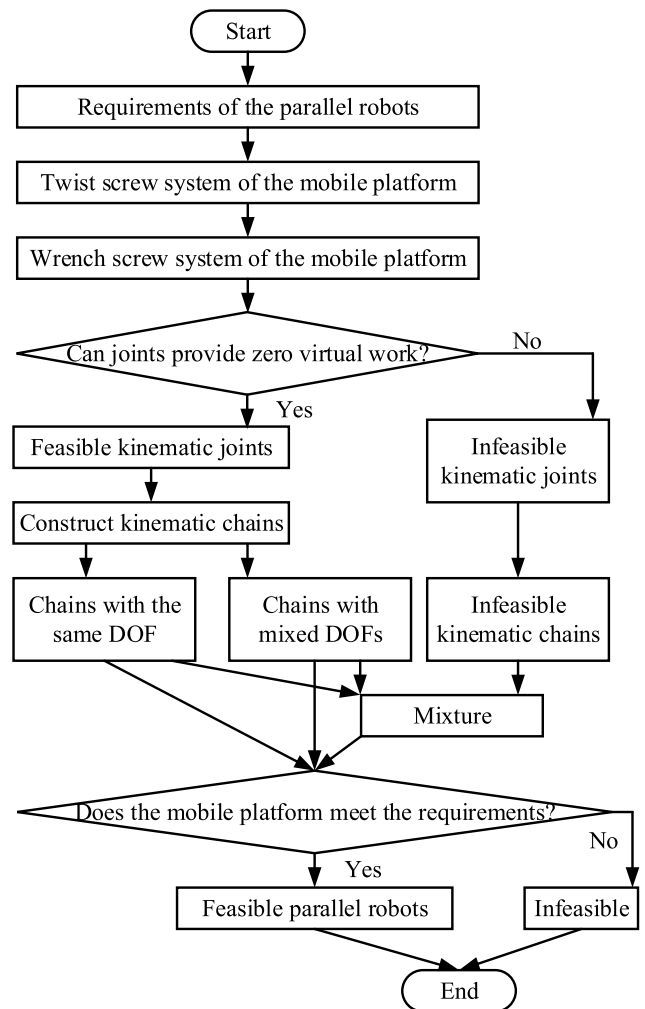
$$OA_5 + A_5A_6 + A_6P = OP \qquad (8)$$

Equation (8) can be further described as below

$$x_{A5}e^{i\theta_3} + L_2e^{i\theta_1} + L_3e^{i\theta_3} + L_6e^{i\theta_3} = x_P + y_Pi \qquad (9)$$

where $\theta_3 = 0$ denote the angle between (OA_5 or A_6A_4 or A_4P or OB_5) and positive X direction, since the offsets along Y axis in Fig. 8 are ignored in calculations.
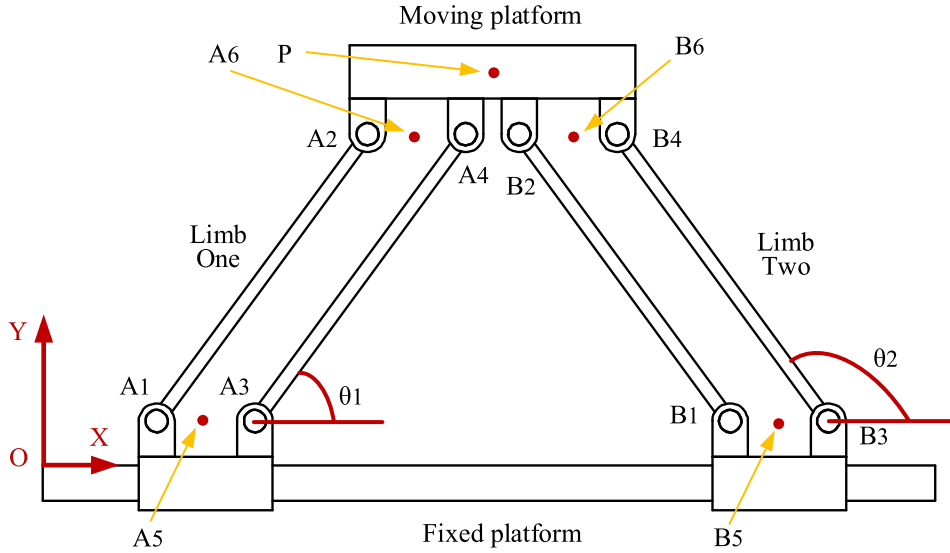
FIGURE 8. Diagram of the translational parallel mechanism.

The sloping angle θ_1 and the position of the first prismatic joint can be calculated as

$$\begin{cases} \theta_1 = \arcsin(y_P/L_2) \\ x_{A5} = x_P - L_3 - L_6 - L_2 \cos\theta_1 \end{cases} \quad (10)$$

The vector-loop formula of the other kinematic limb can be described as

$$OB_5 + B_5B_6 + B_6P = OP \quad (11)$$

Equation (11) can be expressed as

$$x_{B5}e^{i\theta_3} + L_4 e^{i\theta_2} + L_5 e^{i\theta_4} + L_6 e^{i\theta_4} = x_P + y_P i \quad (12)$$

where $\theta_4 = \pi$ is the angle between (B_6B_2 or B_2P) and positive X-axis.

The sloping angle θ_2 and the position of the other prismatic joint can be derived as

$$\begin{cases} \theta_2 = \arcsin(y_P/L_4) \\ x_{B5} = x_{P1} + L_5 + L_6 - L_4 \cos\theta_2 \end{cases} \quad (13)$$

The inverse mathematical solutions are composed of the second equations of (10) and (13).

Rearrange (9) and (12)

$$\Gamma_1 : (x_P - x_{A5} - L_3 - L_6)^2 + y_P^2 - L_2^2 = 0 \quad (14)$$
$$\Gamma_2 : (x_P - x_{B5} + L_5 + L_6)^2 + y_P^2 - L_4^2 = 0 \quad (15)$$

Subtracting (15) from (14) causes

$$L_2^2 - L_4^2 = (x_P - x_{A5} - L_3 - L_6)^2 - (x_P - x_{B5} + L_5 + L_6)^2 \quad (16)$$

The X-value of the dot P of the moving platform can be resolved based on (16)

$$x_P = \frac{(x_{A5} + L_3 + L_6)^2 - (L_5 + L_6 - x_{B5})^2 + L_4^2 - L_2^2}{2(x_{A5} - x_{B5} + L_3 + L_5 + 2L_6)} \quad (17)$$

Combining (14) and (17) yields

$$y_P = \pm\sqrt{L_2^2 - (x_P - x_{A5} - L_3 - L_6)^2} \quad (18)$$

Equations (17) and (18) are the solution for the direct kinematic model of this parallel structure.

IV. KINEMATIC PERFORMANCE EVALUATIONS
A. SINGULARITY ANALYSIS
Taking the first order of (14) and (15) with respect to time yields

$$J_Q[\dot{x}_{A5}, \dot{x}_{B5}]^T = J_X[\dot{x}_P, \dot{y}_P]^T \quad (19)$$

where

$$J_Q = \begin{bmatrix} -(x_P - x_{A5} - L_3 - L_6) & 0 \\ 0 & -(x_P - x_{B5} + L_5 + L_6) \end{bmatrix}$$

$$J_X = \begin{bmatrix} x_P - x_{A5} - L_3 - L_6 & y_P \\ x_P - x_{B5} + L_5 + L_6 & y_P \end{bmatrix}$$

The kinematic Jacobian matrix is formulated as

$$J = J_Q^{-1} J_X \quad (20)$$

Type-I singularity [46], [47] occurs when $Det(J_Q) = 0$. The first scenario is $x_P = x_{A5} + L_3 + L_6$ under the situation that $L_2 \leq L_4$. θ_1 is $\pi/2$ rad in this scenario as depicted in Fig. 9(a). The second scenario is similar with the former. $x_P = x_{B5} - L_5 - L_6$ and θ_2 is $\pi/2$ rad happen when $L_2 \geq L_4$, as indicated in Fig. 9(b). In both scenarios, the moving platform is capable of bearing external force that is collinear with Y axis without driving force.

Type-II singularity happens when $Det(J_X) = 0$. The first solution is $y_P = 0$, which results in two scenarios. In the first case, $\sin\theta_1 = \sin\theta_2 = 0 \& L_2 \neq 0 \& L_4 \neq 0$. Every linkage within this parallel manipulator is parallel to the X axis and Y-direction translation of the moving platform is lost, as presented in Figs. 9(c-e). In the other scenario,
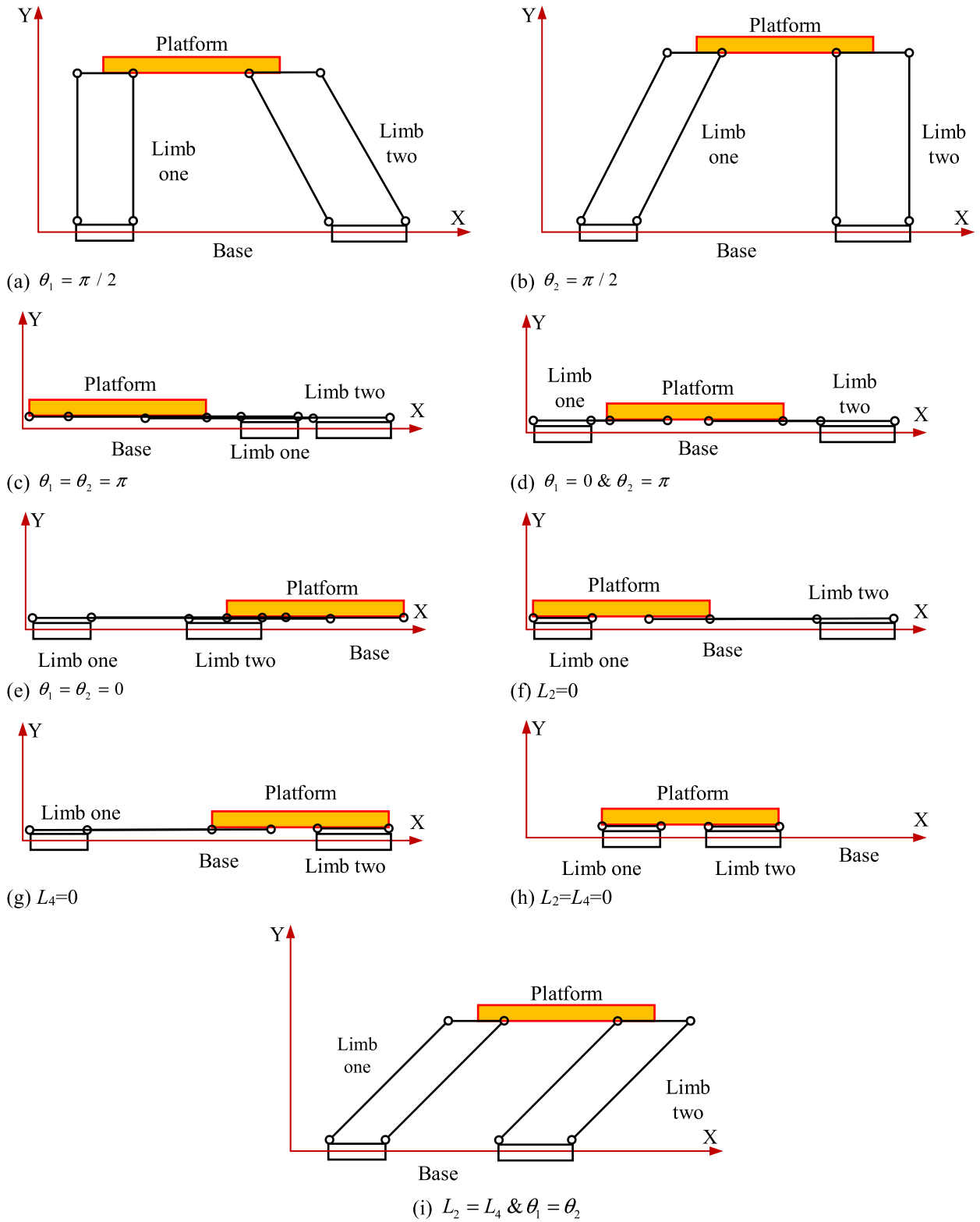
(a) $\theta_1 = \pi / 2$

(b) $\theta_2 = \pi / 2$

(c) $\theta_1 = \theta_2 = \pi$

(d) $\theta_1 = 0 \ \& \ \theta_2 = \pi$

(e) $\theta_1 = \theta_2 = 0$

(f) $L_2 = 0$

(g) $L_4 = 0$

(h) $L_2 = L_4 = 0$

(i) $L_2 = L_4 \ \& \ \theta_1 = \theta_2$

FIGURE 9. Schematic diagram of the singularity configurations.

$L_2 = 0$ or $L_4 = 0$(based on the geometric relationship). The mobile platform owns only one DOF (translation along X direction), as indicated in Figs. 9(f-h). The second solution is $x_{B5} = x_{A5} + L_3 + L_5 + 2L_6$. Combined with (10) and (13), it can be further derived as $L_2 \cos \theta_1 = L_4 \cos \theta_2$. The general result is $L_2 \neq 0 \& L_2 \neq L_4 \& \cos \theta_1 = L_4 \cos \theta_2 / L_2$. A special

case $L_2 = L_4 \& \theta_1 = \theta_2$ is illustrated in Fig.9(i). In this case, the mobile platform is parallel to the X axis, and all sloping linkages in two kinematic chains are parallel. The mobile platform can still move even when two active prismatic joints are fully locked.

The combined singularity occurs when both type-I and type-II conditions are attained. It happens when $L_2 = 0$ or $L_4 = 0$ or $L_2 = L_4 \neq 0 \& \theta_1 = \theta_2 = \pi/2$.

B. WORKSPACE CHARACTERIZATION

The lengths of all linkage are provided as: $L_1 = 195$mm, $L_2 = 100$mm, $L_3 = 22.5$mm, $L_6 = -L_3$ (Two limbs are not in the same plane). $L_3 = L_5$ and $L_2 = L_4$ are utilized to realize the symmetric characteristics of this parallel structure. The ranges of motion for two driving prismatic joints are listed as $L_3 \leq x_{A5} \leq L_1 - 2L_3$ and $2L_3 \leq x_{B5} \leq L_1 - L_3$. The rotational ranges of passive joints are shrunk to avoid the aforementioned singularity configurations and be practical in physical prototype. $\pi/36 \leq \theta_1 \leq 17\pi/36$ and $19\pi/36 \leq \theta_2 \leq 35\pi/36$.
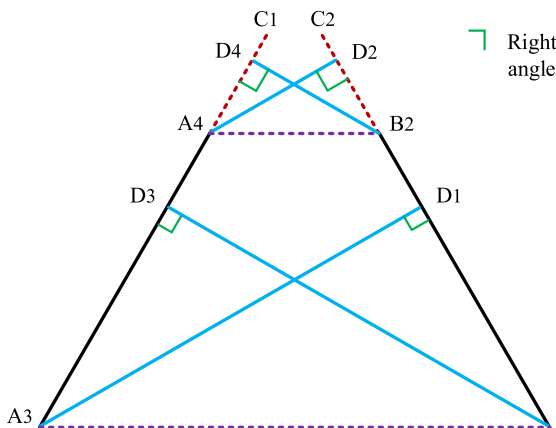

FIGURE 10. Diagram of two adjacent linkages.

Considering the linkage interference [48], two sloping rods in each kinematic chain will not collide based on its geometry. The constraints for rotary joints have already avoided the linkage interference between legs and fixed/moving platform. To prevent the collision between linkages A_1A_3 and B_1B_3, $|x_{B5} - x_{A5}| \geq 2L_3$. Another concern is the interference between linkages A_3A_4 and B_1B_2 if they are assembled in the same plane. It is assumed that both rods are in the cylindrical shape with a diameter of $D_{BAR} = 4$mm. The minimal distance D_{MIN} should meet the following requirement:

$$D_{MIN} \geq D_{BAR} \tag{21}$$

These two linkages are illustrated in Fig. 10. The lines A_4C_1 and B_2C_2 are respectively the extended line of lines A_3A_4 and B_1B_2. Lines A_3D_1 and B_1D_3 are orthogonal with lines A_3A_4 and B_1B_2, respectively. Points D_1 and D_3 are separately on the lines B_1B_2 and A_3A_4. Lines A_4D_2 and B_2D_4 are respectively perpendicular to lines B_2C_2 and A_4C_1, respectively. On the basis of above rotational joint

constraints, rods A_3A_4 and B_1B_2 are not parallel to each other within reachable workspace. Therefore, a line that is perpendicular to and has intersections with both rods does not exist. According to the classifications in [49] and this robot configuration, (21) can be further derived as

$$Min\{|A_4B_2|, |A_3B_1|, |A_3D_1|, |B_1D_3|\} = |A_4B_2| \geq D_{BAR} \tag{22}$$

The position of the mobile platform is given as $x_{A5} < x_P < x_{B5}$, to prevent the singularities discussed in the former section.
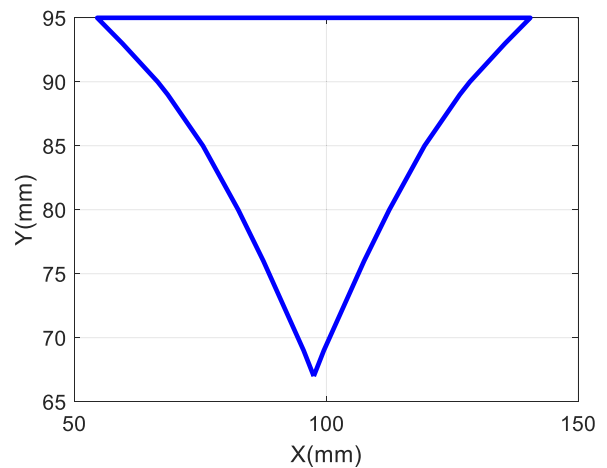

FIGURE 11. Reachable workspace of translational parallel manipulator.

The spatial searching algorithm is employed to identify its reachable workspace, as depicted in Fig. 11. The reachable workspace owns a symmetric shape about $X = 97.5$mm. The workspace region keeps increasing as the height (along Y axis) of the mobile platform rises. It is also noted that the reachable workspace has no hollow parts and is a singularity-free workspace.

C. DEXTERITY ANALYSIS

For this parallel manipulator, its dexterity performance can reveal the transmission relations between two prismatic joints and two translations. The widely used performance indices are condition number and manipulability. Its condition number is utilized in this section. The local condition index (LCI) is computed based on the kinematic Jacobian matrix [50], as expressed below

$$LCI = \|\boldsymbol{J}\|_f \left\|\boldsymbol{J}^{-1}\right\|_f = \frac{(\delta_2 + \delta_3)y_P^2 + 2\delta_2\delta_3}{|y_P|\sqrt{\delta_1\delta_2\delta_3}} \tag{23}$$

where $\|\|_f$ denotes the Frobenius norm and

$$\begin{cases} \delta_1 = (L_2\cos\theta_1 - L_4\cos\theta_2)^2 \\ \delta_2 = L_4^2 - y_P^2 \\ \delta_3 = L_2^2 - y_P^2 \end{cases}$$

It is noted that the performance is not pertinent to x_P according to (23). The passive angles θ_1 and θ_2 are included in (23). They can be eliminated by combining (10) and (13), as provided below

$$LCI = \frac{(\delta_2 + \delta_3)y_P^2 + 2\delta_2\delta_3}{|y_P|\sqrt{(\sqrt{\delta_2} + \sqrt{\delta_3})^2\delta_2\delta_3}} \quad (24)$$

In accordance with (24), LCI is only associated with three variables, y_P, L_2 and L_4. The impacts originated from L_2 or L_4 are the same on this index since these two parameters are interchangeable. Considering the symmetrical structure of this parallel robot, $L_2 = L_4$. This index can be further simplified as

$$LCI = \frac{L_2^2}{|y_P|\sqrt{L_2^2 - y_P^2}} \quad (25)$$

The impacts originated from these two parameters are depicted in Fig. 12. In Fig. 12(a), L_2 is a constant of 100mm. It is shown in Fig. 12(a) that LCI gets smaller as y_P increases and then shows an upward trend since y_P is 71mm. In this scenario, the smallest and largest LCI are 2.0001 and 3.3711, respectively. y_P remains 95mm for Fig. 12(b). Fig. 12(b) indicates LCI displays a downward trend when L_2 becomes longer. The motion transmission capacity is getting better in this process. LCI ranges from 2.0675 to 3.3711 in this scenario. Fig. 12(c) is required to show the overall impacts under all cases of both variables. The range of LCI in this 3D plot is [2, 3.3711]. The maximal LCI is located with the largest y_P and the shortest L_2.

D. KINEMATIC ERROR MODEL

The constraint equation of each limb of a parallel mechanism can be arranged as the following expression,

$$\mathbf{\Gamma}_i(\mathbf{X}, \mathbf{Q}_L, \mathbf{Q}_A) = 0 \quad (26)$$

where $\mathbf{X}$ represents the pose of the moving platform. $\mathbf{Q}_L$ and $\mathbf{Q}_A$ are the linear variables (linkage lengths and linear joint positions) and angular variables (angles of active and passive joints), respectively.

Taking the differential of both sides of (26) with respect to time yields

$$\frac{\partial \mathbf{\Gamma}_i}{\partial \mathbf{X}}\dot{\mathbf{X}} + \frac{\partial \mathbf{\Gamma}_i}{\partial \mathbf{Q}_L}\dot{\mathbf{Q}}_L + \frac{\partial \mathbf{\Gamma}_i}{\partial \mathbf{Q}_A}\dot{\mathbf{Q}}_A = 0 \quad (27)$$
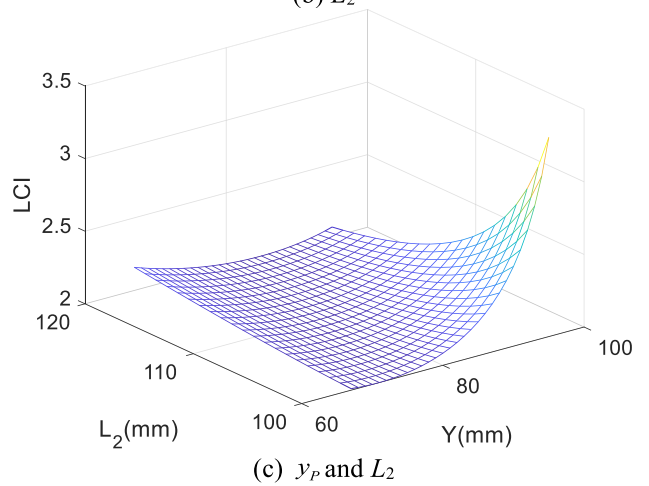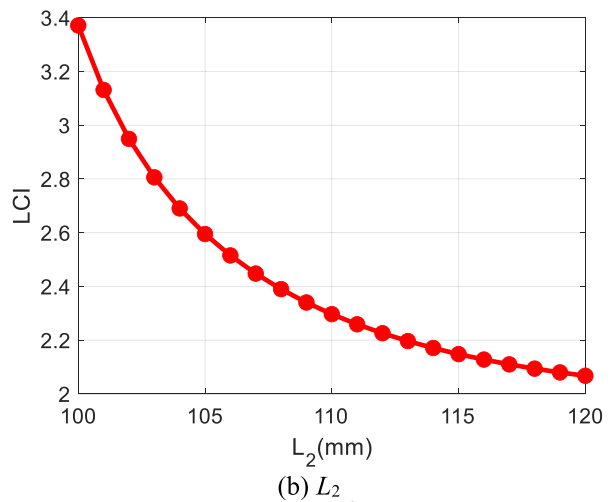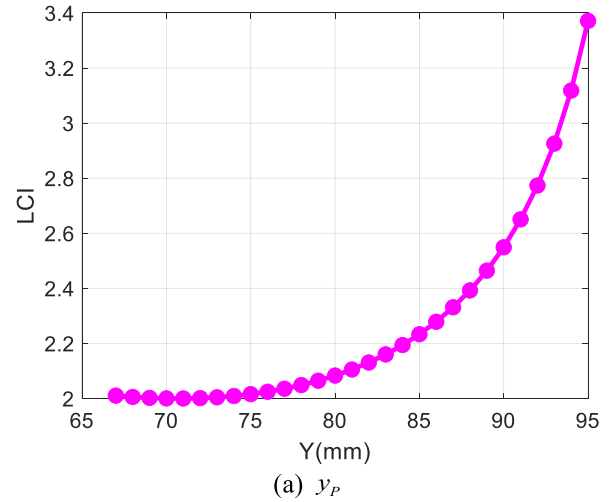
The overall equation set of the parallel manipulator can be arranged as one expression,

$$\mathbf{J}_{XE}\dot{\mathbf{X}} = \mathbf{J}_{LES}\dot{\mathbf{Q}}_L + \mathbf{J}_{AES}\dot{\mathbf{Q}}_A \quad (28)$$

where $\mathbf{J}_{XE}$, $\mathbf{J}_{LES}$ and $\mathbf{J}_{AES}$ respectively indicate the mobile platform pose error, linear error source, angular error source Jacobian matrices.

Equation (28) can be further derived as

$$\dot{\mathbf{X}} = \mathbf{J}_E\dot{\mathbf{Q}}_E = \mathbf{J}_{LE}\dot{\mathbf{Q}}_L + \mathbf{J}_{AE}\dot{\mathbf{Q}}_A \quad (29)$$

(a) y_P

(b) L_2

(c) y_P and L_2

FIGURE 12. Distributions of the local condition index.

where $\mathbf{J}_E$ is the overall error Jacobian matrix. $\mathbf{Q}_E$ includes overall variables (combination of $\mathbf{Q}_L$ and $\mathbf{Q}_A$). The linear error Jacobian matrix $\mathbf{J}_{LE} = \mathbf{J}_{XE}^{-1}\mathbf{J}_{LES}$. The angular error Jacobian matrix $\mathbf{J}_{AE} = \mathbf{J}_{XE}^{-1}\mathbf{J}_{AES}$.

It is noteworthy that linear and angular errors are separated in (26)-(29). This is because there are parallel structures with pure-translation, pure-rotation and mixed-movement (translation and rotation). The separate strategy is utilized for parallel manipulators with mixed motion to avoid non-homogeneous units. The local error condition index (LECI) has been mentioned in much research [51], [52], [53]. When this index approaches 1, every error source tends to have a more equal effect on the pose of the mobile platform. However, the separate linear and angular parameters are not considered. The LECI and two novel indices, local linear error condition index (LLECI) and local angular error condition index (LAECI), are defined below

$$\begin{cases} LECI = \|\boldsymbol{J}_E\| \left\|\boldsymbol{J}_E^{-1}\right\| \\ LLECI = \|\boldsymbol{J}_{LE}\| \left\|\boldsymbol{J}_{LE}^{-1}\right\| \\ LAECI = \|\boldsymbol{J}_{AE}\| \left\|\boldsymbol{J}_{AE}^{-1}\right\| \end{cases} \tag{30}$$

where $\|\ \|$ indicates the matrix norm. It can be Euclidean norm or Frobenius norm. The Euclidean norm is adopted in this section.

The following expression is also provided to overcome the non-square matrix:

$$\begin{cases} LECI = \|\boldsymbol{J}_E\| \left\|\boldsymbol{J}_E^{+}\right\| \\ LLECI = \|\boldsymbol{J}_{LE}\| \left\|\boldsymbol{J}_{LE}^{+}\right\| \\ LAECI = \|\boldsymbol{J}_{AE}\| \left\|\boldsymbol{J}_{AE}^{+}\right\| \end{cases} \tag{31}$$

where the superscript '+' denotes the Moore-Penrose generalized inverse of a matrix.

It is assumed that each parameter in all error sources has the equal contribution (identical magnitude, and same positive or negative value) and all sources are independent. Under this circumstance, every component of $\dot{\boldsymbol{Q}}_E, \dot{\boldsymbol{Q}}_L$ and $\dot{\boldsymbol{Q}}_A$ in (29) are defined as 1, which indicates the overall error performance relies on these error Jacobian matrices. Each row of these Jacobian matrices corresponds to one motion of the mobile platform.

The mobile platform's DOFs range from two to six for a general parallel manipulator. A maximum of six components can denote the motion of the mobile platform, as $\Lambda = [T_X, T_Y, T_Z, R_X, R_Y, R_Z]$. The letter T and R represent translation and rotation, respectively. The corresponding component(s) of this vector can be removed to be consistent with the parallel manipulator owning less than six DOFs. $\boldsymbol{EJ}$ is utilized to represent any error Jacobian matrix mentioned in (29). The size of $\boldsymbol{EJ}$ is $\lambda \times n$ ($2 \leq \lambda \leq 6, n \geq 2$). Three novel error-related indices for any parallel mechanism are developed. The local error coefficient (LEC) is employed to measure the local error performance of any movement (the i-th column represents the i-th DOF of the mobile platform). The local error percentage (LEP) provides the percentage of the local error coefficient of one movement among all error sources. The local error ratio (LER) represents the local error coefficients comparison between any two movements. These

three indices are presented below

$$LEC(\Lambda_i) = \sqrt{\sum_{j=1}^{n} \boldsymbol{EJ}_{i,j}}\ i = 1, 2, \ldots, \lambda \tag{32}$$

$$LEP(\Lambda_i) = \frac{\sqrt{\sum_{j=1}^{n} \boldsymbol{EJ}_{i,j}}}{\sqrt{\sum_{j=1}^{n} \sum_{i=1}^{\lambda} \boldsymbol{EJ}_{i,j}}}\ i = 1, 2, \ldots, \lambda \tag{33}$$

$$LER(\Lambda_i/\Lambda_k) = \frac{\sqrt{\sum_{j=1}^{n} \boldsymbol{EJ}_{i,j}}}{\sqrt{\sum_{j=1}^{n} \boldsymbol{EJ}_{k,j}}}\ i, k = 1, 2, \ldots, \lambda . i \neq k \tag{34}$$

Since the local indicators are associated with the specific configuration of the parallel robot, both the analytical and numerical global indices should be introduced to evaluate the overall performance within workspace. The corresponding global error coefficient (GEC) of any motion, global error percentage (GEP) of any movement and global error ration (GER) between two movements, are derived as

$$GEC(\Lambda_i) = \frac{\int LEC(\Lambda_i)dW}{\int W}$$
$$= \frac{\sum_{\zeta=1}^{SODP} LEC(\Lambda_i)}{SODP}\ i = 1, 2, \ldots, \lambda \tag{35}$$

$$GEP(\Lambda_i) = \frac{\int LEP(\Lambda_i)dW}{\int W}$$
$$= \frac{\sum_{\zeta=1}^{SODP} LEP(\Lambda_i)}{SODP}\ i = 1, 2, \ldots, \lambda \tag{36}$$

$$GER(\Lambda_i/\Lambda_k) = \frac{\int LER(\Lambda_i/\Lambda_k)dW}{\int W}$$
$$= \frac{\sum_{\zeta=1}^{SODP} LER(\Lambda_i/\Lambda_k)}{SODP}$$
$$i, k = 1, 2, \ldots, \lambda . i \neq k \tag{37}$$

where W denotes workspace and SODP is short for sum of discrete poses.

These novel error-related indices are intrinsic characteristics and could provide some primary error evaluations of a parallel structure (especially parallel mechanisms with non-square error Jacobian matrix). i.e., the error impacts from each linkage/joint. They have the potential to assist the linkages dimension optimization. They could help to select a proper parallel architecture for the requirements (if some motions of the mobile platform need high precision, or it is difficult to manufacture precise length of some linkages).

The chosen parallel mechanism is utilized as an example. Equations (14) and (15) are substituted into (26)-(29). The

following expressions are computed

$$J_E = J_{LE} =$$

$$\begin{bmatrix} \eta_1 & y_P \\ \eta_2 & y_P \end{bmatrix}^{-1} \begin{bmatrix} \eta_1 & 0 & L_2 & \eta_1 & 0 & 0 & \eta_1 \\ 0 & \eta_2 & 0 & 0 & L_4 & -\eta_2 & -\eta_2 \end{bmatrix} \quad (38)$$

$$\dot{Q}_E = \dot{Q}_L = \begin{bmatrix} \dot{x}_{A5} & \dot{x}_{B5} & \dot{L}_2 & \dot{L}_3 & \dot{L}_4 & \dot{L}_5 & \dot{L}_6 \end{bmatrix}^{\mathrm{T}} \quad (39)$$

where

$$\begin{cases} \eta_1 = x_P - x_{A5} - L_3 - L_6 \\ \eta_2 = x_P - x_{B5} + L_5 + L_6 \end{cases}$$

The error-related indices of this parallel architecture can be formulated based on (31)-(34). It is worth noticing that these local performance indices are not related to the X component based on calculations. The distribution of LECI is seen in Fig. 13(a). This parallel mechanism has its best LECI when the Y value is 77mm. Its LECI gets worse when the Y value is far away from this special position. From Fig. 13(b), LEC, LEP, LER(T_X/T_Y) keep improving with a larger Y value. From Fig. 13(c), these three performances decrease as Y value reduces gradually. Based on LER indices in Figs. 13(b) and (c), the error along T_X is similar to that along T_Y when Y component of mobile platform is around 77mm. T_Y movement tend to have larger errors than T_X motion before Y-value reaches this point, and the situation is conversed when Y-value is larger than this position. The global indices should be generated in accordance with the whole reachable workspace instead of Figs. 13(b) and (c) due to its irregular shape. According to (35)-(37), the corresponding global indices along T_X movement are 1.8565, 0.8336 and 1.7093, respectively. The global error performances along T_Y movement are separately 1.1585, 0.5305 and 0.6606.

V. EXPERIMENTAL STUDY

The experimental setup of the planar parallel robot is demonstrated in Fig. 14. The linkage lengths of this prototype are provided in Section IV-B. The screw nut system (pitch is 2mm) is applied for the active prismatic joint, which is actuated by the Dynamixel MX-64 servo actuator. The resolution of this motor is 4096 pulse per revolution. The Dynamixel U2D2 [54] is employed to communicate the computer and two motors. A 12-voltage direct current power supply is selected for this robot system.

The desired motion of the moving platform is written as (unit: mm)

$$X = [127.5 + \sin t, 152.95 + (\cos t - 1)]^{\mathrm{T}} \quad (40)$$

where t represents time (unit: second).

Due to the offset of this robot prototype, the required trajectory of the moving platform that is consistent with (10) and (13) is designed as $[110 + \sin t, 90 + (\cos t - 1)]^{\mathrm{T}}$ mm. The mobile platform offsets are 17.5mm for the X axis and 50.95mm for the Y direction, to be applicable for the practical calculations in the physical prototype. The
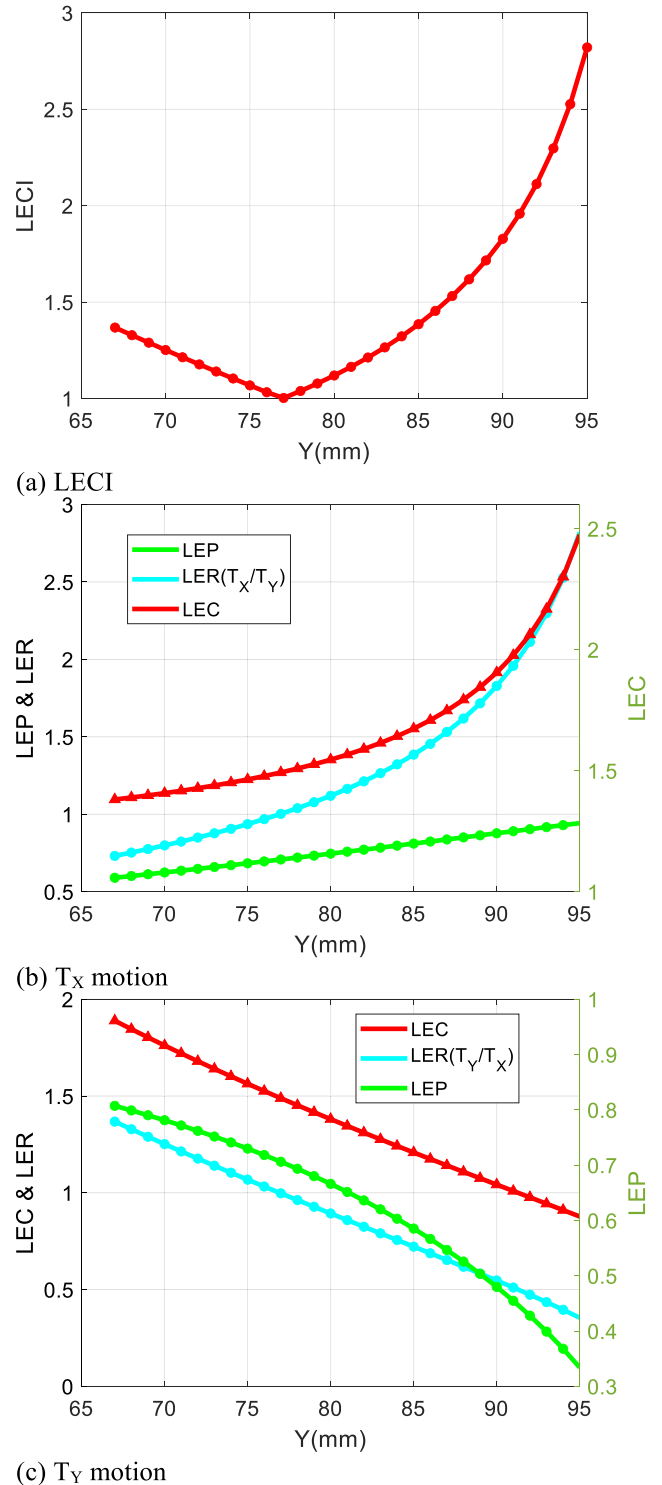

(a) LECI

(b) T_X motion

(c) T_Y motion

FIGURE 13. Distributions of error-related indices.

following computations are derived with the consideration of offsets.

The overall time is set as 2π seconds. There are 73 steps in experiments when the step size is $\pi/36$ seconds. The initial configuration of the moving platform is measured as (127.5, 152.95) mm. According to (10) and (13), the initial
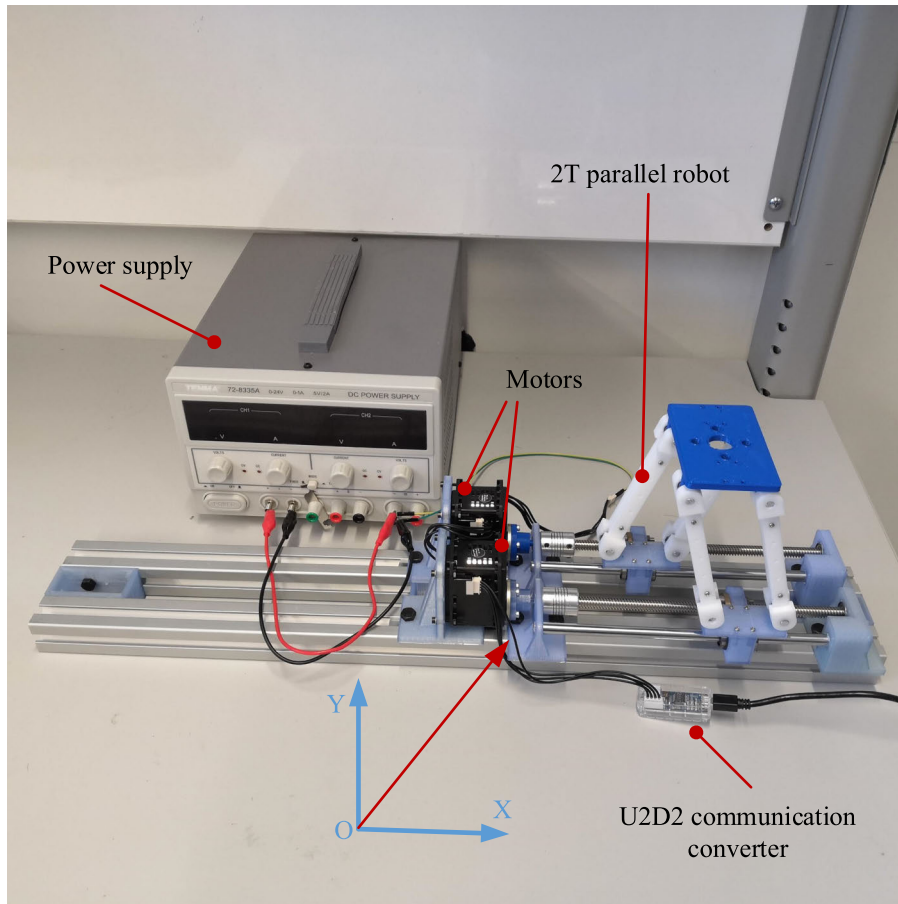
FIGURE 14. The experiential setup of 2T parallel mechanism.

X-components of two active prismatic joints are generated as 83.911 mm and 171.09 mm, respectively. The position of the moving platform can be calculated on the basis of direct kinematic model and encoder data of two actuators.

In the first experiment, the robot runs without controls algorithm and the experimental results are represented in Fig. 15. As seen from Fig. 15(a-b), the experimental trajectory is consistent with the target path, which conforms the kinematic mathematical solutions are correct. The largest movement errors occur when mobile platform runs at the left and right sides of this trajectory. It can be seen from Fig. 15(b) that the absolute position errors along X direction are larger than those in Y direction for most cases. This can be predicted that LER(Tx/Ty) is larger than 1 in Fig. 13(b) or LER(Ty/Tx) is smaller than 1 in Fig. 13(c), when the Y component ranges from 89mm to 91mm. The characteristics of experimental errors are consistent with the distributions in Figs. 13 (b-c). The pulse information of these two prismatic motors is illustrated in Fig. 15(c). The experimental pulses of both motors respectively match with the target pulses. The motion errors of two driving prismatic joints are computed as provided in Fig. 15(d).

The proportional-integral-derivative (PID) control strategy is employed to enable the minimal motion differences in the

second experiment. PID control scheme is convenient and owns high reliability and good robustness [55]. Two PID controllers in joint space are constructed for this parallel robot. The positions of two actuating joints are measured and the motion errors are expressed as

$$\begin{cases} e_1(t) = \text{desired} x_{A5} - \text{actual} x_{A5} \\ e_2(t) = \text{desired} x_{B5} - \text{actual} x_{B5} \end{cases} \tag{41}$$

The i-th ($i = 1,2$) controller output is defined as

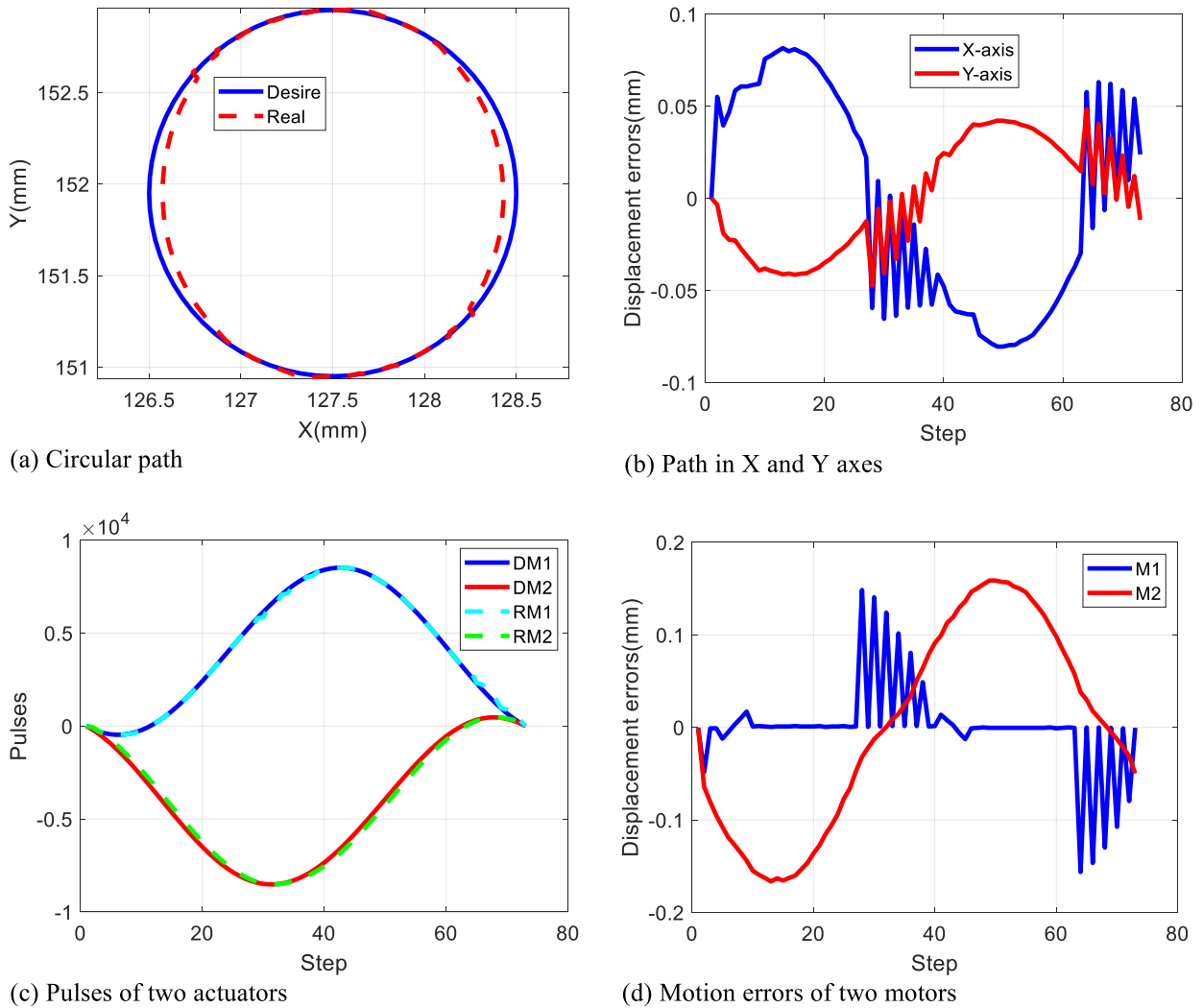$$u_i(t) = K_{Pi}e_i(t) + K_{Ii}\int e_i(t)dt + K_{Di}\frac{de_i(t)}{dt} \tag{42}$$

where K_{Pi}, K_{Ii} and K_{Di} respectively represent the i-th proportional, integral and derivative variables.

The positions of two prismatic joints serving as the controlled parameters are employed to foster the proposed parallel robot to approach the desired trajectory smoothly and accurately. The parameters of two controllers are selected through the trial-and-error method, as listed below

$$\begin{cases} K_{P1} = 9 & K_{I1} = 0 & K_{D1} = 4.5 \\ K_{P2} = 9.01 & K_{I2} = 18.34 & K_{D2} = 5.45 \end{cases} \tag{43}$$

Both the target and experimental motions of the mobile platform are indicated in Fig. 16(a). The movement errors

(a) Circular path

(b) Path in X and Y axes

(c) Pulses of two actuators

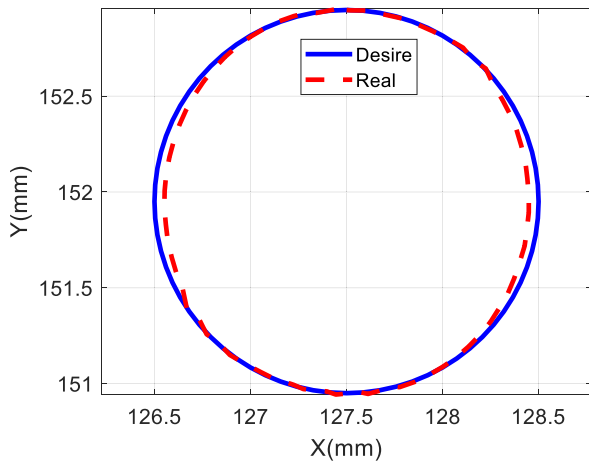(d) Motion errors of two motors

FIGURE 15. The experiment results under no-controller (D and R separately mean desired and real results. M1 and M2 respectively denote Motor 1 and Motor 2).

**TABLE 3.** RMSE comparisons between two experiments.

Cases	Mobile platform			Motors	
	X-axis	Y-axis	Overall position	Motor 1	Motor 2
No controller	0.0588	0.0305	0.0662	0.0469	0.1087
PID control	0.0422	0.0246	0.0489	0.0289	0.0857

along X-axis and Y-axis are further formulated and displayed in Fig. 16(b). The pulse data of both motors is shown in Fig. 16(c) and the position errors for two driving prismatic joints are demonstrated in Fig. 16(d). Additional quantitative comparison of two scenarios is provided in Table 3. The root mean squared error (RMSE) is used to compute the closeness of mobile platform trajectory and displacements of active prismatic joints. As shown in Figs. 15(a-b) and Figs. 16(a-b) and Table 3, this moving platform trajectory with control algorithm is closer to the desired trajectory. In the latter case, the motion errors along both orthogonal directions are reduced and this case is more stable due to less sawtooth waves. As demonstrated in Fig. 15(c) and Fig. 16(c)
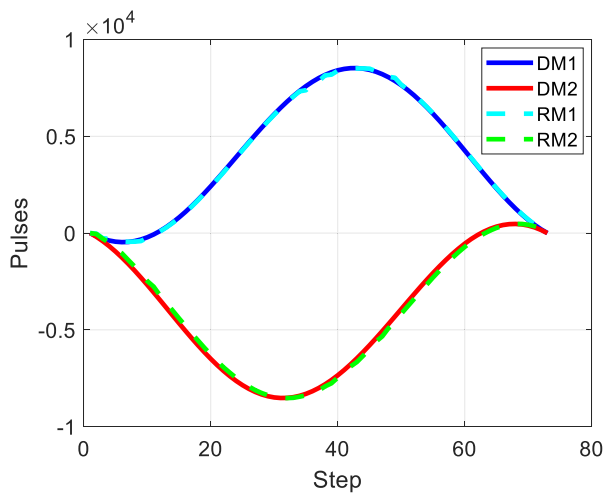
and Table 3, the experimental results of two motors in the latter scenario respectively have better closeness with the desired pulses, compared with the situation without controller. The errors in Fig. 16(d) for both prismatic joints are shrunk under PID control method through comparing with the results demonstrated in Fig. 15(d) and Table 3. These motion errors are small compared with the intentional trajectory. The position errors of moving platform and actuators can be further noticeably mitigated with machined parts when compared with the low-cost 3-dimensional printed rods. Overall, the designed PID control strategy can achieve the desired path smoothly and accurately.
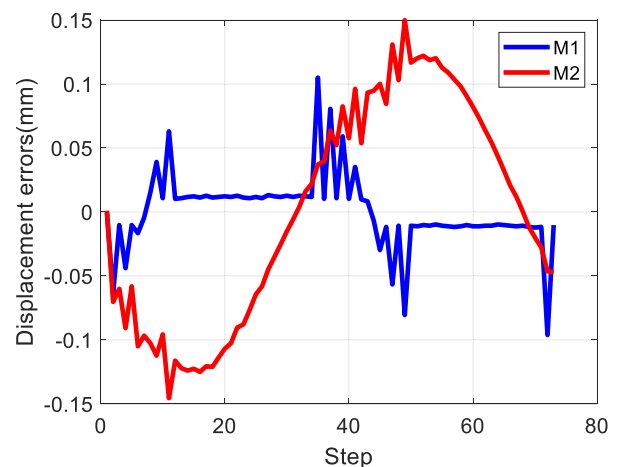
(a) Circular path
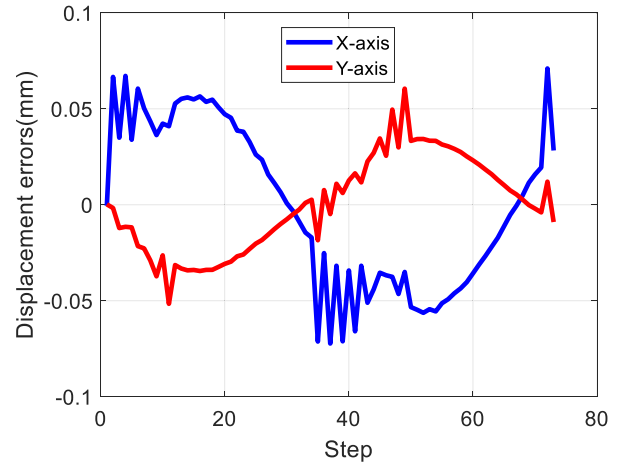
(b) Path in X and Y axes

(c) Pulses of two actuators

(d) Motion errors of two motors

FIGURE 16. The experiment results under PID controller (D and R separately mean desired and real results. M1 and M2 respectively denote Motor 1 and Motor 2)m.

VI. CONCLUSION

(1) A detailed structural synthesis approach based on screw theory for a class of 2T parallel mechanisms is described in this paper. The promising kinematic joints and limbs are explored according to the constraints of the mobile platform and 28 practical parallel structures are generated in total. The predefined mobile platform and fixed base assist to gain the possibility for additional six supporting limbs which are infeasible based on the preliminary calculations. A subgroup of 42 parallel manipulators constituting of unqualified kinematic chains are developed by taking advantage of the promising kinematic branches.

(2) A symmetrical parallel architecture is selected and detailed mathematical position models are constructed. The local condition index is formulated and is not related to the X position. Its distribution is explored with reference to the Y position and linkage length L_2 (or L_4). The novel LLECI and LAECI are defined to separate linear and angular

variables and achieve homogeneous units. In accordance with a general kinematic error model for parallel manipulator, three novel indices, LEC, LEP and LER are introduced for performance assessments as well as their corresponding global indices. These indices are applicable for overall, linear and angular error Jacobian matrices for general parallel mechanisms. These indices of the selected mechanism are explored. The correctness of kinematic mathematical models and the distributions of local error ratio indices are testified by experiments.

(3) The dynamic performance analysis and optimal design will be incorporated into the future work. The selected parallel robot has the potential as a picking-and-placing robot for heavy products considering the large workspace and high payload capacity originated from planar kinematic pairs. A hybrid design (e.g., 5-DOF P(2-PPa)RR. The first P joint is normal to the plane of 2-PPa. The orthogonal RR serial configuration is a 2-DOF rotating head) can

be constructed for enhanced workspace and more flexible grasping operations.

REFERENCES

[1] B. Siciliano and O. Khatib, *Springer Handbook of Robotics*. Berlin, Germany: Springer, 2008.

[2] M. Luces, J. K. Mills, and B. Benhabib, "A review of redundant parallel kinematic mechanisms," *J. Intell. Robotic Syst.*, vol. 86, no. 2, pp. 175–198, May 2017.

[3] B. Belzile, P. K. Eskandary, and J. Angeles, "Workspace determination and feedback control of a pick-and-place parallel robot: Analysis and experiments," *IEEE Robot. Autom. Lett.*, vol. 5, no. 1, pp. 40–47, Jan. 2020.

[4] M. Stock and K. Miller, "Optimal kinematic design of spatial parallel manipulators: Application to linear delta robot," *J. Mech. Design*, vol. 125, no. 2, pp. 292–301, Jun. 2003.

[5] S. Zarkandi, "Dynamic modeling and power optimization of a 4RPSP+PS parallel flight simulator machine," *Robotica*, vol. 40, no. 3, pp. 646–671, Mar. 2022.

[6] H. Fang, T. Tang, Z. He, Y. Liu, and J. Zhang, "A novel hybrid machine tool integrating a symmetrical redundantly actuated parallel mechanism: Design, kinematics, prototype and experiment," *Mechanism Mach. Theory*, vol. 176, Oct. 2022, Art. no. 105013.

[7] D. Zhang, Y. Zheng, L. Wei, J. Wu, Y. Xu, and Y. Zhao, "Type synthesis of 2T1R planar parallel mechanisms and their moduling development applications," *IEEE Access*, vol. 9, pp. 72217–72227, 2021.

[8] P. Lambert and J. L. Herder, "A 7-DOF redundantly actuated parallel haptic device combining 6-DOF manipulation and 1-DOF grasping," *Mechanism Mach. Theory*, vol. 134, pp. 349–364, Apr. 2019.

[9] W.-A. Cao, S.-J. Xu, K. Rao, and T. Ding, "Kinematic design of a novel two degree-of-freedom parallel mechanism for minimally invasive surgery," *J. Mech. Design*, vol. 141, no. 10, Oct. 2019, Art. no. 104501.

[10] C. Qiu and J. S. Dai, *Analysis and Synthesis of Compliant Parallel Mechanisms-Screw Theory Approach*. Berlin, Germany: Springer International Publishing, 2021.

[11] Q. Li, J. M. Hervé, and W. Ye, *Geometric Method for Type Synthesis of Parallel Manipulators*. Singapore: Springer, 2020.

[12] J. Wei and J. S. Dai, "Reconfiguration-aimed and manifold-operation based type synthesis of metamorphic parallel mechanisms with motion between 1R2T and 2R1T," *Mechanism Mach. Theory*, vol. 139, pp. 66–80, Sep. 2019.

[13] A. Antonov, A. Fomin, V. Glazunov, D. Petelin, and G. Filippov, "Type synthesis of 5-DOF hybrid (Parallel-Serial) manipulators designed from open kinematic chains," *Robotics*, vol. 12, no. 4, p. 98, Jul. 2023.

[14] H. Shen, Y. Zhao, G. Wu, J. Li, and D. Chablat, "Kinematic design of a translational parallel mechanism based on sub-kinematic chain determined workspace superposition," in *Proc. Inst. Mech. Eng. Part C, J. Mech. Eng. Sci.*, vol. 235, no. 24, pp. 7534–7549, Dec. 2021.

[15] T. Tang, H. Fang, H. Luo, Y. Song, and J. Zhang, "Type synthesis, unified kinematic analysis and prototype validation of a family of exechon inspired parallel mechanisms for 5-axis hybrid kinematic machine tools," *Robot. Comput.-Integr. Manuf.*, vol. 72, Dec. 2021, Art. no. 102181.

[16] Y. Liu, Y. Li, Y.-A. Yao, and X. Kong, "Type synthesis of multi-mode mobile parallel mechanisms based on refined virtual chain approach," *Mechanism Mach. Theory*, vol. 152, Oct. 2020, Art. no. 103908.

[17] Y. Xu, Y. Zhao, Y. Yue, F. Xi, J. Yao, and Y. Zhao, "Type synthesis of overconstrained 2R1T parallel mechanisms with the fewest kinematic joints based on the ultimate constraint wrenches," *Mechanism Mach. Theory*, vol. 147, May 2020, Art. no. 103766.

[18] G. Jia, H. Huang, S. Wang, and B. Li, "Type synthesis of plane-symmetric deployable grasping parallel mechanisms using constraint force parallelogram law," *Mechanism Mach. Theory*, vol. 161, Jul. 2021, Art. no. 104330.

[19] B.-J. Yi and W. K. Kim, "Task-oriented type synthesis of the lower-mobility parallel mechanisms with a common platform," *J. Mech. Sci. Technol.*, vol. 32, no. 11, pp. 5373–5387, Nov. 2018.

[20] A. Fomin, A. Antonov, and S. Kiselev, "A new class of foldable mechanisms with a circular rail—FoldRail mechanisms," *Mech. Mach. Theor.*, vol. 189, Nov. 2023, Art. no. 105425.

[21] S. Patel and T. Sobh, "Manipulator performance measures–A comprehensive literature survey," *J. Intell. Robotic Syst.*, vol. 77, nos. 3–4, pp. 547–570, Mar. 2015.

[22] C. Chen and J. Angeles, "Generalized transmission index and transmission quality for spatial linkages," *Mechanism Mach. Theory*, vol. 42, no. 9, pp. 1225–1237, Sep. 2007.

[23] Y. Zhao, J. Wang, Y. Cao, B. Liang, and T. Zhao, "Constant motion/force transmission analysis and synthesis of a class of translational parallel mechanisms," *Mechanism Mach. Theory*, vol. 108, pp. 57–74, Feb. 2017.

[24] C. Gosselin and L.-T. Schreiber, "Redundancy in parallel mechanisms: A review," *Appl. Mech. Rev.*, vol. 70, no. 1, Jan. 2018, Art. no. 010802.

[25] D. Wang, R. Fan, and W. Chen, "Performance enhancement of a three-degree-of-freedom parallel tool head via actuation redundancy," *Mechanism Mach. Theory*, vol. 71, pp. 142–162, Jan. 2014.

[26] P. Cardou, S. Bouchard, and C. Gosselin, "Kinematic-sensitivity indices for dimensionally nonhomogeneous Jacobian matrices," *IEEE Trans. Robot.*, vol. 26, no. 1, pp. 166–173, Feb. 2010.

[27] T. Do Thanh, J. Kotlarski, B. Heimann, and T. Ortmaier, "On the inverse dynamics problem of general parallel robots," in *Proc. IEEE Int. Conf. Mechatronics*, Apr. 2009, pp. 1–6.

[28] J. Brinker, B. Corves, and Y. Takeda, "Kinematic performance evaluation of high-speed delta parallel robots based on motion/force transmission indices," *Mechanism Mach. Theory*, vol. 125, pp. 111–125, Jul. 2018.

[29] J. P. Merlet, "Jacobian, manipulability, condition number, and accuracy of parallel robots," *J. Mech. Design*, vol. 128, no. 1, pp. 199–206, Jan. 2006.

[30] W. A. Khan and J. Angeles, "The kinetostatic optimization of robotic manipulators: The inverse and the direct problems," *J. Mech. Design*, vol. 128, no. 1, pp. 168–178, Jan. 2006.

[31] M. Chen, Q. Zhang, X. Qin, and Y. Sun, "Kinematic, dynamic, and performance analysis of a new 3-DOF over-constrained parallel mechanism without parasitic motion," *Mechanism Mach. Theory*, vol. 162, Aug. 2021, Art. no. 104365.

[32] X.-J. Liu, X. Chen, and M. Nahon, "Motion/Force constrainability analysis of lower-mobility parallel manipulators," *J. Mech. Robot.*, vol. 6, no. 3, Aug. 2014, Art. no. 031006.

[33] Q. Meng, F. Xie, X.-J. Liu, and Y. Takeda, "Screw theory-based motion/force transmissibility analysis of high-speed parallel robots with articulated platforms," *J. Mech. Robot.*, vol. 12, no. 4, Aug. 2020, Art. no. 041011.

[34] E. Sharafian M, A. Taghvaeipour, and M. Ghassabzadeh S, "Revisiting screw theory-based approaches in the constraint wrench analysis of robotic systems," *Robotica*, vol. 40, no. 5, pp. 1406–1430, May 2022.

[35] Q. Xu and Y. Li, "An investigation on mobility and stiffness of a 3-DOF translational parallel manipulator via screw theory," *Robot. Comput.-Integr. Manuf.*, vol. 24, no. 3, pp. 402–414, Jun. 2008.

[36] T. Sun, T. Wu, B. Lian, Y. Qi, P. Wang, and Y. Song, "Stiffness modeling, analysis and evaluation of a 5 degree of freedom hybrid manipulator for friction stir welding," in *Proc. Inst. Mech. Eng. Part C, J. Mech. Eng. Sci.*, vol. 231, no. 23, pp. 4441–4456, Dec. 2017.

[37] H. Qi, G. Liwen, and W. Jianxin, "Dynamic performance evaluation of a 2-DoF planar parallel mechanism," *Int. J. Adv. Robotic Syst.*, vol. 9, no. 6, p. 250, Dec. 2012.

[38] X.-J. Liu, J. Wang, and G. Pritschow, "Performance atlases and optimum design of planar 5R symmetrical parallel mechanisms," *Mechanism Mach. Theory*, vol. 41, no. 2, pp. 119–144, Feb. 2006.

[39] T. Huang, Z. Li, M. Li, D. G. Chetwynd, and C. M. Gosselin, "Conceptual design and dimensional synthesis of a novel 2-DOF translational parallel robot for pick-and-place operations," *J. Mech. Design*, vol. 126, no. 3, pp. 449–455, May 2004.

[40] X. Yang, L. Zhu, Y. Ni, H. Liu, W. Zhu, H. Shi, and T. Huang, "Modified robust dynamic control for a diamond parallel robot," *IEEE/ASME Trans. Mechatronics*, vol. 24, no. 3, pp. 959–968, Jun. 2019.

[41] J. Wu, J. Wang, T. Li, and L. Wang, "Analysis and application of a 2-DOF planar parallel mechanism," *J. Mech. Design*, vol. 129, no. 4, pp. 434–437, Apr. 2007.

[42] X.-J. Liu, J. Li, and Y. Zhou, "Kinematic optimal design of a 2-degree-of-freedom 3-parallelogram planar parallel manipulator," *Mechanism Mach. Theory*, vol. 87, pp. 1–17, May 2015.

[43] X.-J. Liu, Q.-M. Wang, and J. Wang, "Kinematics, dynamics and dimensional synthesis of a novel 2-DoF translational manipulator," *J. Intell. Robotic Syst.*, vol. 41, no. 4, pp. 205–224, Jan. 2005.

[44] V. B. N. Pham and H. S. Kim, "Dynamics analysis of a 2-DOF planar translational parallel manipulator," *J. Korean Soc. Manuf. Technol. Engineers*, vol. 22, no. 2, pp. 185–191, Apr. 2013.

[45] Y. Fang and L.-W. Tsai, "Enumeration of a class of overconstrained mechanisms using the theory of reciprocal screws," *Mechanism Mach. Theory*, vol. 39, no. 11, pp. 1175–1187, Nov. 2004.

[46] I. A. Bonev, D. Zlatanov, and C. M. Gosselin, "Singularity analysis of 3-DOF planar parallel mechanisms via screw theory," *J. Mech. Design*, vol. 125, no. 3, pp. 573–581, Sep. 2003.

[47] Q. Zou, "Type synthesis and performance optimization of parallel manipulators," TPh.D. dissertation, Dept. Mech. Eng., Univ., Toronto, Toronto, ON, Canada, 2022.

[48] C. Gosselin and L.-T. Schreiber, "Kinematically redundant spatial parallel mechanisms for singularity avoidance and large orientational workspace," *IEEE Trans. Robot.*, vol. 32, no. 2, pp. 286–300, Apr. 2016.

[49] O. Masory and J. Wang, "Workspace evaluation of stewart platforms," *Adv. Robot.*, vol. 9, no. 4, pp. 443–461, Jan. 1994.

[50] L. J. Puglisi, R. J. Saltaren, H. A. Moreno, P. F. Cárdenas, G. Garcia, and R. Aracil, "Dimensional synthesis of a spherical parallel manipulator based on the evaluation of global performance indexes," *Robot. Auto. Syst.*, vol. 60, no. 8, pp. 1037–1045, Aug. 2012.

[51] Y. Ni, N. Wu, X. Zhong, and B. Zhang, "Dimensional synthesis of a 3-DOF parallel manipulator with full circle rotation," *Chin. J. Mech. Eng.*, vol. 28, no. 4, pp. 830–840, Jul. 2015.

[52] S. Qian, B. Zi, D. Zhang, and L. Zhang, "Kinematics and error analysis of cooperative cable parallel manipulators for multiple mobile cranes," *Int. J. Mech. Mater. Design*, vol. 10, no. 4, pp. 395–409, Dec. 2014.

[53] B. Zi, H. Ding, X. Wu, and A. Kecskeméthy, "Error modeling and sensitivity analysis of a hybrid-driven based cable parallel manipulator," *Precis. Eng.*, vol. 38, no. 1, pp. 197–211, Jan. 2014.

[54] L. Bao, D. Kim, S.-J. Yi, and J. Lee, "Design of a sliding mode controller with fuzzy rules for a 4-DOF service robot," *Int. J. Control, Autom. Syst.*, vol. 19, no. 8, pp. 2869–2881, Aug. 2021.

[55] M. W. Spong and M. Vidyasagar, *Robot Dynamics and Control*. Hoboken, NJ, USA: Wiley, 2008.

DAN ZHANG (Senior Member, IEEE) received the Ph.D. degree in mechanical engineering from Laval University, Canada, in 2000.

He is currently a Chair Professor in intelligent robotics and automation with The Hong Kong Polytechnic University. He joined Ontario Tech University (OTU), Canada, as an Assistant Professor, in 2004, and was promoted to an Associate Professor and a Professor, in 2006 and 2011, respectively. During the appointment period with OTU, he was the Founding Chair of the Department of Automotive, Mechanical and Manufacturing Engineering (2012–2014) and was awarded the Canada Research Chair in Advanced Robotics and Automation (2009–2015). Since 2016, he has been transferring to York University, Canada, as a Kaneff Professor and also took up the role of the Department Chair of the Department of Mechanical Engineering, from 2016 to 2018. Thereafter, he was awarded the Tier 1 York Research Chair in Advanced Robotics and Mechatronics, in 2017. His research interests include synthesis and optimization of parallel and hybrid mechanisms, generalized parallel mechanisms research, reconfigurable robots, and innovation design of parallel robots: parallelization of serial robots, micro/nano manipulation and mems devices (e.g., sensors), rescue robots, smart biomedical instruments (e.g., exoskeleton robots and rehabilitation robotics), AI/robotics/autonomous systems, aerial and underwater robotics, artificial intelligence for robotics, and intelligent reconfigurable adaptive landing gear and manipulator (manipulander).

Prof. Zhang is a fellow of the Canadian Academy of Engineering (CAE), the Engineering Institute of Canada (EIC), the American Society of Mechanical Engineers (ASME), and the Canadian Society for Mechanical Engineering (CSME); and a Senior Member of SME.

QI ZOU received the bachelor's and master's degrees from Beijing Jiaotong University, in 2016 and 2019, respectively, and the Ph.D. degree in mechanical engineering from York University, in 2023. Currently, he is a Postdoctoral Fellow in electrical engineering with Hanyang University. His research interests include type synthesis, kinematic, and dynamic analysis of parallel robotics.

YUANCHENG SHI received the bachelor's and master's degrees from Pusan National University, South Korea, in 2018 and 2020, respectively. He is currently pursuing the Ph.D. degree with the Department of Electrical Engineering, Hanyang University. From 2020 to 2021, he was an Engineer with Hikvision. His research interests include robotics and medical robot.

BYUNG-JU YI (Member, IEEE) received the B.S. degree in mechanical engineering from Hanyang University, Seoul, Republic of Korea, in 1984, and the M.S. and Ph.D. degrees in mechanical engineering from The University of Texas at Austin, Austin, TX, USA, in 1986 and 1991, respectively. From 1991 to 1992, he was a Postdoctoral Fellow with the Robotics Group, The University of Texas at Austin. From 1992 to 1995, he was an Assistant Professor with the Department of Mechanical and Control Engineering, Korea Institute of Technology and Education, Cheonan-si, Chungcheongnam-do, Republic of Korea. In 1995, he joined the Department of Control and Instrumentation Engineering, Hanyang University. He was a Visiting Professor with Johns Hopkins University, Baltimore, MA, USA, in 2004. He was a JSPS Fellow with Kyushu University, Japan, in 2011. He is currently a Professor with the Department of Electrical and Electronic Engineering, Hanyang University. His research interests include general robot mechanics with application to surgical robotic systems (ENT, neurosurgical, and needle insertion areas), deep learning-based robotic manipulation, and ubiquitous sensor network-based robotics. He is a member of the IEEE Robotics and Automation Society. From 2005 to 2008, he was an Associate Editor of IEEE TRANSACTIONS ON ROBOTICS. He was the President of the Korean Robotics Society and the Korean Society of Medical Robotics.

GUANYU HUANG received the bachelor's and Ph.D. degrees from Beijing Jiaotong University, in 2013 and 2018, respectively. He has been an Associate Researcher with the Zhejiang Laboratory, since 2019. His research interests include design and control of parallel, biped, and other robots.

• • •